

Rayleigh-Taylor instability of viscoelastic self-rewetting film flowing down a temperature-controlled inclined substrate

Siyi An(安思亦) and Yongjun Jian(菅永军)

Citation: Chin. Phys. B, 2023, 32 (**6**): 064701. DOI: 10.1088/1674-1056/acc78b
Journal homepage: http://cpb.iphy.ac.cn; http://iopscience.iop.org/cpb

What follows is a list of articles you may be interested in

Lattice Boltzmann model for interface capturing of multiphase flows based on Allen-Cahn equation

He Wang(王贺), Fang-Bao Tian(田方宝), and Xiang-Dong Liu(刘向东)
Chin. Phys. B, 2022, 31 (**2**): 024701. DOI: 10.1088/1674-1056/ac11d8

A simplified approximate analytical model for Rayleigh-Taylor instability in elastic-plastic solid and viscous fluid with thicknesses

Xi Wang(王曦), Xiao-Mian Hu(胡晓棉), Sheng-Tao Wang(王升涛), and Hao Pan(潘昊)
Chin. Phys. B, 2021, 30 (**4**): 044702. DOI: 10.1088/1674-1056/abcf44

Interface coupling effects of weakly nonlinear Rayleigh-Taylor instability with double interfaces

Zhiyuan Li(李志远), Lifeng Wang(王立锋), Junfeng Wu(吴俊峰), Wenhua Ye(叶文华)
Chin. Phys. B, 2020, 29 (**3**): 034704. DOI: 10.1088/1674-1056/ab6965

Investigation of convergent Richtmyer-Meshkov instability at tin/xenon interface with pulsed magnetic driven imploding

Shaolong Zhang(张绍龙), Wei Liu(刘伟), Guilin Wang(王贵林), Zhengwei Zhang(章征伟), Qizhi Sun(孙奇志), Zhaohui Zhang(张朝辉), Jun Li(李军), Yuan Chi(池原), Nanchuan Zhang(张南川)
Chin. Phys. B, 2019, 28 (**4**): 044702. DOI: 10.1088/1674-1056/28/4/044702

Wetting failure condition on rough surfaces

Feng-Chao Yang(杨冯超), Xiao-Peng Chen(陈效鹏)
Chin. Phys. B, 2019, 28 (**4**): 044701. DOI: 10.1088/1674-1056/28/4/044701

Rayleigh–Taylor instability of viscoelastic self-rewetting film flowing down a temperature-controlled inclined substrate

Siyi An(安思亦) and Yongjun Jian(菅永军)†

School of Mathematical Science, Inner Mongolia University, Hohhot 010021, *China*

(Received 30 October 2022; revised manuscript received 19 February 2023; accepted manuscript online 25 March 2023)

Rayleigh–Taylor (RT) instability of gravity-driven viscoelastic self-rewetting film flowing under an inclined substrate uniformly heated or cooled is considered. The surface tension of self-rewetting film is considered as a quadratic function of temperature. The long wave hypothesis is used to derive a nonlinear free surface evolution equation of the thin viscoelastic film. Linear stability analysis shows that for a prescribed the viscoelastic coefficient, substrate cooling products instability, while substrate heating remains stability. Furthermore, we analyze the influence of viscoelastic coefficient on RT instability. Results show that the viscoelastic coefficient reinforces the RT instability whether the substrate is heated or cooled. Moreover, we use the line method to numerically simulate the nonlinear evolution equation and systematically examine the space-time variation of the film free surface. The numerical results illustrate that increasing the viscoelastic coefficient can enhance the disturbance amplitude and wave frequency. This means that the viscoelastic coefficient makes the system unstable, which is consistent with result of the linear stability analysis. In addition, the oscillation tends to accumulate downstream of the inclined substrate when the evolution time is long enough. Finally, the variation of film thickness with related parameters for different viscoelastic coefficients is investigated.

Keywords: Rayleigh–Taylor instability, self-rewetting film, viscoelastic liquid

PACS: 47.20.Ma, 47.15.gm, 47.50.–d **DOI:** 10.1088/1674-1056/acc78b

1. Introduction

The Rayleigh–Taylor (RT) instability describes the destabilization of the interface separating stratified fluids under the action of a gravitative acceleration directed from the heavier fluid towards the lighter fluid. In other words, it occurs when a heavier fluid layer is supported from below in the gravity field by a lighter one.[1–3] RT instability, as a basic interface phenomenon, is applied in many aspects, such as solid substrate undersurface coating,[4] liquid polymer film flow,[5] the dynamics of rain drops and their role in the biosphere,[6] in micro fluidics and lab-on-a-chip technology,[7] as well as in nature, such as the formation of mushroom clouds from volcanic eruptions and fingerlike patterns in granular flows.[8] Excellent reviews on the RT instability were given by Sharp[9] and Kull.[10] In many applications, however, RT instability, such as the instability may lead to coating irregularities or to the detachment of droplets for thick coatings, is an undesirable event. Therefore, controlling and suppressing RT instability is very important in a variety of engineering applications. This can be achieved, for example, by exploiting an electric field,[11] a high-frequency mechanical oscillation,[12] a rotating magnetic field,[13] spatial confinement,[14] and enlarging surface tension gradients.[15] In addition to these strategies, considering the influence of fluid characteristics on this instability is also an approach worth exploring.

The literature is rich in the analysis of RT instability of thin film flows in the case of Newtonian fluid.[16,17] Yiantsios and Higgins[18] focused on the asymptotic analysis of RT instability in thin viscous films with horizontal substrates. Afterwards, Brun *et al.*[19] discussed this problem on an inclined plane and revealed that no drops form for inclinations greater than a critical value. The nonlinear dynamics of pendent drops on a thin film coating the underside of a ceiling was studied by Lister *et al.*,[20] and in the absence of other complexities, the competition between surface tension and gravity leads to instability. More recently, Chao *et al.*[21] investigated how the thermocapillary stress controls or modifies the RT instability of a gravity-driven viscous liquid film in the case of an inclined substrate. They found that the thermocapillary stress in the heated film enhances the absolute instability and inhibits the convective instability, while the trend is opposite for the cooled film. It is worth noting that in all the above-mentioned studies, the RT instability problem was analyzed for a Newtonian liquid layer.

However, in many applications, we deal with fluids that exhibit non-Newtonian behavior. For example, in blood and mucus, the shear stress of its fluid is a nonlinear function of the local strain rate, which causes it to behave in violation of Newton laws. Viscoelastic fluid, as a non-Newtonian fluid, has typical characteristics of Newton fluid (viscosity) and solid (elasticity). A polymer liquid consisting of a Newtonian (viscous) solvent and a non-Newtonian (polymeric) solute is a

†Corresponding author. E-mail: jianyj@imu.edu.cn

© 2023 Chinese Physical Society and IOP Publishing Ltd

typical example of a viscoelastic fluid. There are many kinds of constitutive models of viscoelastic fluid, such as Maxwell model,[22] Jeffrey model,[23] Giesekus model,[24] Phan Thien Tanner model,[25] Oldroyd model,[26] *etc*. In these models, the elastic nature of the fluid is measured using a relaxation time. Boffetta *et al.*[27] and Gou *et al.*[28] studied RT instability of Oldroyd-B model and Maxwell model respectively. Detailed linear theoretical and numerical analyses have shown that elasticity destabilizes a system when viscoelasticity is present. Among these models, the most frequently used model in practical is Walters B″,[29] whose constitutive equation involves only a non-Newtonian parameter. The stability of a thin film of Walters B″ viscoelastic fluid flowing down a heated inclined plane is investigated by Fu *et al*.[30] They used normal mode analysis to determine the instability threshold, and studied the effects of the Marangoni number, viscoelastic parameter, and Biot number. At the same time, the authors found that the instability of the thin film was enhanced by viscoelasticity and thermocapillarity under prescribed conditions. In addition, the reduction of Marangoni number leads to shrinkage of the film instability region, which is also demonstrated by the authors. It is worth noting that the authors reported that the accuracy of their model decreases as the Marangoni number increases. Walters B″ liquid finds its usage in medicinal diagnosis and clinical applications.[31–33] Apart from these, viscoelastic film has important significance in lubrication and coating processes,[34] drag reduction process,[35] and liquid lining flows in airways.[36]

It is noteworthy that in all the above-mentioned RT instability studies, the surface tension is usually assumed to be a linear function of temperature. However, self-rewetting fluid,[37] such as the dilute aqueous solutions of long-chain alcohols, has a quadratic temperature dependence of surface tension. For a self-rewetting fluid, the surface tension grows stronger with temperature when the temperature exceeds a critical value. Karapetsas *et al.*[38] studied the diffusion of a self-rewetting droplet on a non-uniformly heated horizontal substrate and they concentrated on the influence of wettability variation on drop movement. Mamalis *et al.*[39] experimentally investigated the situation of a self-rewetting droplet deposited on a uniformly heated, horizontal substrate in a partially wetting condition. Ye *et al.*[40] further studied the effects of the inclination angle, capillary number, Bond number, and thermocapillary force on the migration of the self-rewetting drop under the condition of uniform substrate heating. They found that nonmonotonic dependence of interfacial tension on temperature had an important influence on drop spreading. Recently, there are few studies concerning instability of self-rewetting films on temperature-controlled tilted substrate. Batson *et al.*[41] established a thin liquid film evolution equation for quadratic surface tension by using long-wave approximation, which generated an unstable hot capillary driving force. The dynamics of the film flow was numerically analyzed and linear stability analysis was given to obtain the critical conditions. Ma and Liu[42] examined the evolution patterns and essential mechanisms of flow instability of a self-rewetting fluid coating on an inclined plane. Using the thin-film model, the evolution equation of the air–liquid interface was derived, and numerical result showed that when the interfacial temperature smaller than temperature corresponding to the minimum of surface tension, the Marangoni effect enhances the fingering instability. On the contrary, the Marangoni effect makes the flow more stable. All these results indicated that the self-rewetting fluid shows a similar phenomenon to that of a normal fluid before exceeding a critical temperature, because the surface tension of both self-rewetting fluid and ordinary fluids exhibits a negative gradient in this situation. Exceeding a certain temperature, the self-rewetting fluid indicates a positive gradient surface tension and the flow instability will be crucially affected.

However, the study of the RT instability of viscoelastic self-rewetting film on a temperature-controlled inclined substrate is needed to be investigated. Most of the current works are associated with Newtonian self-rewetting film. In order to further understand the non-Newtonian self-rewetting liquid both in theory and in possible future experiment, we will study viscoelastic self-rewetting film. In this work, we aim to examine the RT instability of the viscoelastic self-rewetting film flowing down a temperature-controlled inclined substrate and to reveal how these parameters influence the flow instability. The rest of this paper is structured as follows. In Section 2, we formulate the physical model of the problem and derive a nonlinear partial differential equation for the thickness of viscoelastic self-rewetting film. In Sections 3–5, we systematically examine the linear stability, the nonlinear traveling wave, and the transient simulation of evolution equation in the absence/presence of viscoelastic coefficient, respectively. Conclusions of this work are drawn in Section 6.

2. Mathematical description

2.1. Governing equations and boundary conditions

Consider an inclined substrate with a uniform and constant temperature T_s and length L, beneath which an incompressible thin viscoelastic self-rewetting film flows, as shown in Fig. 1. Here, T_s is generally not equal to the ambient gas temperature T_g. The inclination angle of the substrate from

the horizontal is defined as α, where $\alpha = 0$ corresponds to the horizontal case. The rheological model of the viscoelastic liquid in the layer is described by the Walters B$''$ liquid. To provide a description of the flow system, we choose a two-dimensional Cartesian coordinate system (x,z), where x and z coordinates are in the directions along and normal to the solid substrate, respectively. The ambient gas is passive and inviscid so that its motion is neglected. The thickness of the film at any instant t is denoted by $h(x,t)$, with an unperturbed thickness of h_0. It is supposed that the variations of the density ρ and the viscosity μ within the fluid due to temperature differences are both negligible.[43]

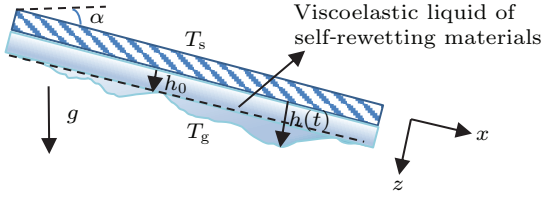


Fig. 1. Schematic representation of a self-rewetting viscoelastic fluid flowing down an inclined plate with constant temperature.

The proposed model represents an approximation to the first order in elasticity and obeys constitutive equation given by Beard and Walters[44]

$$\pi_{ij} = -p\delta_{ij} + 2\mu e_{ij} - 2\gamma_0 \frac{\delta e_{ij}}{\delta t}, \tag{1}$$

where π_{ij} is the stress tensor, p is the isotropic pressure, δ_{ij} is the Kronecker delta, γ_0 is the viscoelastic coefficient, $e_{ij} = (\partial u_j/\partial x_i + \partial u_i/\partial x_j)/2$ is the rate of strain tensor, and u_i are the components of the velocity in the x_i direction of a fixed coordinate system. When the viscoelastic coefficient γ_0 is set to zero, the constitutive equation (1) recovers the Newtonian situation. The co-rotational derivative of the rate of strain tensor $\delta e_{ij}/\delta t$ is defined as

$$\frac{\delta e_{ij}}{\delta t} = \frac{\partial e_{ij}}{\partial t} + u_m \frac{\partial e_{ij}}{\partial x_m} - \frac{\partial u_j}{\partial x_m} e_{im} - \frac{\partial u_i}{\partial x_m} e_{mj}. \tag{2}$$

Motion of the laminar, incompressible, weakly viscoelastic liquid film is governed by the continuity equation and momentum equation, which are represented in vector form as

$$\nabla \cdot \boldsymbol{u} = 0, \tag{3}$$

$$\rho\left(\frac{\partial}{\partial t} + (\boldsymbol{u}\cdot\nabla)\right)\boldsymbol{u} = \rho\boldsymbol{g} + \nabla\cdot\pi, \tag{4}$$

where $\nabla = (\partial/\partial x, \partial/\partial z)$ is the gradient operator, $\boldsymbol{u} = (u,w)$ denotes the velocity vector, $\boldsymbol{g} = (g\sin\alpha, g\cos\alpha)$ is the gravity acceleration, and π is the Cauchy stress tensor whose components are given in Eqs. (1) and (2). Since the viscous dissipation effect is very small in our present parametric regions, so it is ignored in energy equation. Temperature T within the liquid phase is governed by

$$\rho c_p \frac{DT}{Dt} = \lambda \nabla^2 T. \tag{5}$$

Here, λ and c_p denoting the thermal conductivity and the specific heat capacity of the liquid, respectively.

At $z = 0$, no-slip, no-penetration boundary conditions, and a constant surface temperature at the inclined wall are

$$u = 0, \quad w = 0, \quad T = T_s. \tag{6}$$

The balances of normal stresses and of shear stresses at the liquid-air interface $z = h(x,t)$ yield, respectively,

$$\boldsymbol{n}\cdot\boldsymbol{\pi}\cdot\boldsymbol{n} = -k\sigma, \tag{7}$$

$$\boldsymbol{n}\cdot\boldsymbol{\pi}\cdot\boldsymbol{t} = \nabla_s\sigma\cdot\boldsymbol{t}, \tag{8}$$

where $\boldsymbol{n} = 1/(1+\partial^2 h/\partial x^2)^{1/2}(-\partial h/\partial x, 1)$ is the unit normal vector, $\boldsymbol{t} = 1/(1+\partial^2 h/\partial x^2)^{1/2}(1, \partial h/\partial x)$ is the unit tangent vector, and $\boldsymbol{\sigma}$ is the surface tension of the liquid–air interface. For self-rewetting fluids, the surface tension $\boldsymbol{\sigma}$ is often modeled as a quadratic function of temperature T, given by

$$\sigma = \sigma_0 + \sigma_T (T - T_0)^2, \tag{9}$$

where σ_0 is the minimal surface tension attained at $T = T_0$, and $\sigma_T = (1/2)\mathrm{d}^2\sigma/\mathrm{d}T^2$ is the positive surface tension parameter.[37] Its physical properties with ordinary fluids are shown in Fig. 2.

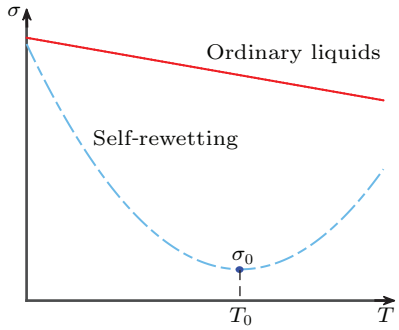


Fig. 2. Physical property of an ordinary fluid and a self-rewetting fluid.

At the liquid–air interface $z = h(x,t)$, the heat transfer between the liquid and the ambient gas is given by the Newton's law of cooling[45]

$$-\lambda \frac{\partial T}{\partial \boldsymbol{n}} = h_g (T - T_g), \tag{10}$$

where h_g is the rate of convective heat transfer from the liquid to the ambient gas. The system is closed by imposing the kinematic boundary condition at $z = h(x,t)$, which reads

$$h_t + u h_x - w = 0. \tag{11}$$

The components of the Cauchy stress tensor $\boldsymbol{\pi}$ obtained from Eqs. (1) and (2) are presented as

$$\pi_{xx} = -p + 2\mu u_x - 2\gamma_0 [u_{xt} + u u_{xx} + w u_{xz}$$

$$-2u_x^2-u_z(u_z+w_x)], \tag{12a}$$

$$\pi_{zz} = -p+2\mu w_z-2\gamma_0[w_{zt}+ww_{zz}+uw_{xz} -2w_z^2-w_x(u_z+w_x)], \tag{12b}$$

$$\pi_{xz} = \pi_{zx}=\mu(u_z+w_x)-\gamma_0[u_{zt}+w_{xt}+u(w_{xx}+u_{xz}) +w(w_{xz}+u_{zz})-2(u_zw_z+u_xw_x)]. \tag{12c}$$

Without further explanation, the subscripts of all variables below represent relevant partial derivatives. Substituting formula (12), the governing equations (3) and (4) can be rewritten as follows:

$$u_x+w_z=0, \tag{13a}$$

$$u_t+uu_x+wu_z=g\sin\alpha-\frac{1}{\rho}p_x+\frac{\mu}{\rho}(u_{xx}+u_{zz}) -\frac{\gamma_0}{\rho}(u_{xxt}+u_{zzt}-3u_xu_{xx}+uu_{xxx}+wu_{xxz}-uw_{zzz} +wu_{zzz}+w_{zz}u_z+2w_xw_{zz}-u_zw_{xx}-w_zu_{zz}), \tag{13b}$$

$$w_t+uw_x+ww_z=g\cos\alpha-\frac{1}{\rho}p_z+\frac{\mu}{\rho}(w_{xx}+w_{zz}) -\frac{\gamma_0}{\rho}(w_{xxt}+w_{zzt}-3w_zw_{zz}+ww_{zzz}+uw_{xzz}-wu_{xxx} +uw_{xxx}-w_{xx}u_x+2u_zu_{xx}-w_xu_{zz}-w_xu_{xx}), \tag{13c}$$

$$T_t+uT_x+wT_z=K(T_{xx}+T_{zz}), \tag{13d}$$

where $K=\lambda/\rho c_{\rm p}$ is the thermal diffusivity of the liquid.

Boundary conditions are expressed as

$$u=0,\quad w=0,\quad T=T_{\rm s},\ \text{ at }\ z=0, \tag{14}$$

and at the free interface $z=h(x,t)$ are

$$-p+\frac{2\mu}{1+h_x^2}[(h_x^2-1)u_x-h_x(u_z+w_x)]+4\gamma_0u_x^2 -\frac{2\gamma_0}{1+h_x^2}\{(h_x^2-1)(u_{xt}+u_zw_x-ww_{zz}-uu_{xx}) -h_x^2u_z^2+w_x^2-h_x[u_{zt}+w_{xt}+u(w_{xx}-w_{zz})+w(u_{zz}-u_{xx}) -2u_zw_z-2u_xw_x]\}=\frac{\sigma}{(1+h_x^2)^{3/2}}h_{xx}, \tag{15a}$$

$$\frac{\mu}{1+h_x^2}[(1-h_x^2)(u_z+w_x)+2h_x(w_z-u_x)] +\frac{1}{1+h_x^2}\{2\gamma_0h_x(2u_{xt}+2uu_{xx}+2ww_{zz}-u_z^2+w_x^2-2u_zw_x) -(1-h_x^2)\gamma_0[u_{zt}+w_{xt}+u(w_{xx}-w_{zz})+w(u_{zz}-u_{xx}) -2(u_zw_z+u_xw_x)]\}=\frac{1}{(1+h_x^2)^{1/2}}\frac{\partial\sigma}{\partial T}(T_x+h_xT_z), \tag{15b}$$

$$-\frac{\lambda}{(1+h_x^2)^{1/2}}(-h_xT_x+T_z)=h_{\rm g}(T-T_{\rm g}). \tag{15c}$$

2.2. Nondimensionalization

To write the governing equations as well as the boundary conditions in dimensionless form, we apply the following set of scaling:

$$(u,w)=U_0(U,W),$$

$$(x,z,h)=h_0(X,Z,H),\quad p=\frac{\mu U_0}{h_0}P,$$

$$t=\frac{h_0}{U_0}\tau,\quad T-T_{\rm g}=(T_{\rm s}-T_{\rm g})\theta,\quad \gamma=\frac{\gamma_0}{\rho h_0^2}, \tag{16}$$

where $U_0=\rho gh_0^2\sin\alpha/\mu$ is the characteristic velocity, given by the balance between the x component of gravity and the viscous force, and $T_{\rm s}-T_{\rm g}$ is the characteristic temperature, defined as the temperature difference between the substrate surface and the ambient gas.

Using the above dimensionless variables, the scaled governing equations are obtained as

$$U_X+W_Z=0, \tag{17a}$$

$$Re(U_\tau+UU_X+WU_Z)=1-P_X+U_{XX}+U_{ZZ} -\gamma Re(U_{XX\tau}+U_{ZZ\tau}-3U_XU_{XX}+UU_{XXX}+WU_{XXZ} -UW_{ZZZ}+WU_{ZZZ}+W_{ZZ}U_Z +2W_XW_{ZZ}-U_ZW_{XX}-W_ZU_{ZZ}), \tag{17b}$$

$$Re(W_\tau+UW_X+WW_Z)=\cot\alpha-P_Z+W_{XX}+W_{ZZ} -\gamma Re(W_{XX\tau}+W_{ZZ\tau}-3W_ZW_{ZZ}+WW_{ZZZ}+UW_{XZZ} -WU_{XXX}+UW_{XXX}-W_{XX}U_X +2U_ZU_{XX}-W_XU_{ZZ}-W_XU_{XX}), \tag{17c}$$

$$Pe(\theta_\tau+U\theta_X+W\theta_Z)=\theta_{XX}+\theta_{ZZ}, \tag{17d}$$

where the Reynolds number, $Re=\rho U_0h_0/\mu$, determines the ratio of inertial to viscous forces, and the Péclet number, $Pe=RePr$, characterizes the ratio of convection to diffusion, with the Prandtl number $Pr=\mu/\rho K$ measuring the ratio of momentum to thermal diffusivities.

The boundary conditions in non-dimensional form are given by

$$U=0,\quad W=0,\quad \theta=1,\ \text{ at }\ Z=0, \tag{18}$$

and at $Z=H(X,\tau)$

$$-P+\frac{2}{1+H_X^2}[(H_X^2-1)U_X-H_X(U_Z+W_X)] +4Re\gamma U_X^2-\frac{2Re\gamma}{1+H_X^2} \times\{(H_X^2-1)(U_{X\tau}+U_ZW_X-WW_{ZZ}-UU_{XX}) -H_X^2U_Z^2+W_X^2-H_X[U_{Z\tau}+W_{X\tau}+U(W_{XX}-W_{ZZ}) +W(U_{ZZ}-U_{XX})-2U_ZW_Z-2U_XW_X] =\left[We+\frac{1}{2}Ma(\theta_{\rm i}-\theta_0)^2\right]\frac{H_{XX}}{(1+H_X^2)^{3/2}}, \tag{19a}$$

$$\frac{1}{\sqrt{1+H_X^2}}[(1-H_X^2)(U_Z+W_X)+2H_X(W_Z-U_X)] +\frac{Re\gamma}{\sqrt{1+H_X^2}}\{2H_X(2U_{X\tau}+2UU_{XX}+2WW_{ZZ}-U_Z^2$$

$$+W_X^2-2U_ZW_X)-(1-H_X^2)[U_{Z\tau}+W_{X\tau}+U(W_{XX}-W_{ZZ})$$
$$+W(U_{ZZ}-U_{XX})-2(U_ZW_Z+U_XW_X)]\}$$
$$=Ma(\theta_{\rm i}-\theta_0)(\theta_{{\rm i}_X}+H_X\theta_{{\rm i}_Z}), \tag{19b}$$
$$\frac{1}{\sqrt{(1+H_X^2)}}(\theta_{{\rm i}_Z}-H_X\theta_{{\rm i}_X})=-Bi\theta_{\rm i}, \tag{19c}$$
$$H_\tau+UH_X-W=0, \tag{19d}$$

where a new variable, $\theta_{\rm i}$, is adopted to denote the temperature at the liquid–gas interface, the Weber number $We=\sigma_0/\mu U_0$ determines the ratio of capillary to viscous forces, the Marangoni number $Ma=2\sigma_{\rm T}(T_{\rm s}-T_{\rm g})^2/\mu U_0$ indicates the ratio of thermocapillary to viscous forces, and the Biot number $Bi=h_{\rm g}h_0/\lambda$ quantifies the ratio of the conduction resistance of the liquid film to the interfacial resistance. It should also be noted that $\theta_{\rm i}$ is nonconstant and it is a function of X, Z, H. For normal films, the Marangoni term is determined by the interfacial temperature, $\theta_{\rm i}$ (see Eq. (13) in Ref. [46]). However, for self-rewetting films, it is determined by the difference between the interfacial temperature $\theta_{\rm i}$ and θ_0 (see Eq. (19b) or Eq. (12b) in Ref. [47]). Here, $\theta_0=(T_0-T_{\rm g})/(T_{\rm s}-T_{\rm g})$ is the dimensionless temperature at which the surface tension obtains its minimal value.

2.3. Long-wave approximation

Referring to the long wave model, the interfacial slope, temporal and spatial fluctuations of the thin film are very slow, resulting in the introduction of a film parameter, $\varepsilon=h_0/L\sim\partial_\tau\sim\partial_X\ll 1$. We use the following approximation to rescale:

$$(\partial_\tau,\partial_X)\to\varepsilon(\partial_\tau,\partial_X),\quad \partial_{XX}\to\varepsilon^2\partial_{XX},\quad W\to\varepsilon W. \tag{20}$$

After inserting Eq. (20) into Eqs. (17)–(19), the governing equations become

$$U_X+W_Z=0, \tag{21a}$$
$$\varepsilon Re(U_\tau+UU_X+WU_Z)$$
$$=1-\varepsilon P_X+\varepsilon^2U_{XX}+U_{ZZ}-\gamma Re(\varepsilon^3U_{XX\tau}+\varepsilon U_{ZZ\tau}$$
$$-3\varepsilon^3U_XU_{XX}+\varepsilon^3UU_{XXX}+\varepsilon^3WU_{XXZ}-\varepsilon UW_{ZZZ}$$
$$+\varepsilon WU_{ZZZ}+\varepsilon W_{ZZ}U_Z+2\varepsilon^3W_XW_{ZZ}$$
$$-\varepsilon^3U_ZW_{XX}-\varepsilon W_ZU_{ZZ}), \tag{21b}$$
$$\varepsilon^2Re(W_\tau+UW_X+WW_Z)$$
$$=\cot\alpha-P_Z+\varepsilon^3W_{XX}+\varepsilon W_{ZZ}-\gamma Re(\varepsilon^4W_{XX\tau}+\varepsilon^2W_{ZZ\tau}$$
$$-3\varepsilon^2W_ZW_{ZZ}+\varepsilon^2WW_{ZZZ}+\varepsilon^2UW_{XZZ}-\varepsilon^4WU_{XXX}$$
$$+\varepsilon^4UW_{XXX}-\varepsilon^4W_{XX}U_X+2\varepsilon^2U_ZU_{XX}$$
$$-\varepsilon^2W_XU_{ZZ}-\varepsilon^4U_{XX}W_X), \tag{21c}$$
$$\varepsilon Pe(\theta_\tau+U\theta_X+W\theta_Z)=\varepsilon^2\theta_{XX}+\theta_{ZZ}. \tag{21d}$$

Boundary conditions are

$$U=0,\quad W=0,\quad \theta=1,\ \text{at}\ Z=0. \tag{22}$$

On the free surface, we only consider $O(H_x)$ terms whereas other higher-order terms, such as $O(H_x^2)$, are ignored. So the boundary conditions at $Z=H(X,\tau)$ are

$$-P-2\varepsilon[U_X+H_X(U_Z+\varepsilon^2W_X)]+4Re\gamma\varepsilon^2U_X^2$$
$$+2Re\gamma\varepsilon^2\{U_{X\tau}+U_ZW_X-WW_{ZZ}-UU_{XX}$$
$$-\varepsilon^2W_X^2+H_X[U_{Z\tau}+\varepsilon^2W_{X\tau}+U(\varepsilon^2W_{XX}-W_{ZZ})$$
$$+W(U_{ZZ}-\varepsilon^2U_{XX})-2U_ZW_Z-2\varepsilon^2U_XW_X]\}$$
$$=[We+\frac{1}{2}Ma(\theta_{\rm i}-\theta_0)^2]\varepsilon^2H_{XX}, \tag{23a}$$
$$U_Z+\varepsilon^2W_X+2\varepsilon^2H_X(W_Z-U_X)+Re\gamma\{2\varepsilon^3H_X(2U_{X\tau}$$
$$+2UU_{XX}+2WW_{ZZ}-\varepsilon^{-2}U_Z^2+\varepsilon^2W_X^2$$
$$-2U_ZW_X)-\varepsilon[U_{Z\tau}+\varepsilon^2W_{X\tau}+U(\varepsilon^2W_{XX}-W_{ZZ})$$
$$+W(U_{ZZ}-\varepsilon^2U_{XX})-2(U_ZW_Z+\varepsilon^2U_XW_X)]\}$$
$$=Ma(\theta_{\rm i}-\theta_0)\varepsilon(\theta_{{\rm i}_X}+H_X\theta_{{\rm i}_Z}), \tag{23b}$$
$$\theta_{{\rm i}_Z}-\varepsilon^2H_X\theta_{{\rm i}_X}=-Bi\theta_{\rm i}, \tag{23c}$$
$$H_\tau+UH_X-W=0. \tag{23d}$$

Here, we consider a typical self-rewetting fluid, the water-1-butanol 5 vol% (volume of 4 μl) with $\rho=10^3$ kg/m^3, $\mu=10^{-3}$ Pa·s–10^{-4} Pa·s, $\sigma\approx 3\times10^{-2}$ N/m, and surface-tension parameter $\sigma_{\rm T}\approx 2.2\times10^{-6}$ N/mK. The parameters in the present simulation are computed from the experiments conducted by Mamalis *et al.*[48] Given by the temperature difference of $T_{\rm s}-T_{\rm g}\approx 10$ K and the characteristic velocity U_0 of 10^{-1} m/s, we can estimate that Re is from 1 to 10, We is from 100 to 1000, Ma is from 0 to 4,[49] Bi is from 0.01 to 1.[40] Further, we assume $Pr\ll 1$, so the convective heat transfer term is neglected in the energy Eq. (21d).

To get the asymptotic solutions of Eqs. (21)–(23), we expand the velocity components U, W, pressure P and the absolute temperature θ asymptotically in powers of aspect ratio $\varepsilon(\ll 1)$ as follows:

$$U=U^0+\varepsilon U^1+{\rm O}(\varepsilon^2),\quad W=W^0+\varepsilon W^1+{\rm O}(\varepsilon^2),$$
$$P=P^0+\varepsilon P^1+{\rm O}(\varepsilon^2),\quad \theta=\theta^0+\varepsilon\theta^1+{\rm O}(\varepsilon^2), \tag{24}$$

where $[U^0,\ W^0,\ P^0,\ \theta^0]$ and $[U^1,\ W^1,\ P^1,\ \theta^1]$ are the leading-order and the first-order solutions, respectively. It should be pointed out that the flow dynamics of the higher-order $O(\varepsilon^2)$ will be ignored in the following analysis in Eq. (24).

We substitute Eq. (24) into the governing Eq. (21) as well as the boundary conditions (22)–(23) and solve these equations up to $O(\varepsilon)$. The zeroth-order solutions of velocity pro-

files along X, Z directions, pressure distributions and temperature profile

$$U^0 = -\frac{1}{2}Z^2 + HZ, \tag{25a}$$

$$W^0 = -\frac{1}{2}H_X Z^2, \tag{25b}$$

$$P^0 = \cot\alpha(Z-H) - \varepsilon^2 WeH_{XX} - \frac{1}{2}Ma(\theta_{\rm i}^0-\theta_0)^2\varepsilon^2 H_{XX}, \tag{25c}$$

$$\theta^0 = 1 - \frac{BiZ}{1+BiH}, \tag{25d}$$

where the leading-order interfacial temperature is therefore obtained as $\theta_{\rm i}^0 = \theta^0|_{Z=H} = 1/(1+BiH)$.

For the first-order problems, the U^1 and P^1 are calculated as

$$\begin{aligned} U^1 = {} & \left[\cot\alpha H_X + \varepsilon^2 WeH_{XXX} + \frac{1}{2}Ma(\theta_{\rm i}^0-\theta_0)^2\varepsilon^2 H_{XXX} \right. \\ & \left. + Ma(\theta_{\rm i}^0-\theta_0)\theta_{{\rm i}X}^0\varepsilon^2 H_{XX}\right]\left(HZ - \frac{Z^2}{2}\right) \\ & + Ma(\theta_{\rm i}^0-\theta_0)\theta_{{\rm i}X}^0 Z + Re\left(\frac{Z^3}{6}H_\tau - \frac{Z}{2}H^2H_\tau \right. \\ & \left. - \frac{Z}{6}H^4H_X + \frac{Z^4}{24}HH_X\right) \\ & - Re\gamma\left(\frac{Z^2}{2}HH_X - H_\tau Z - 2H^2H_X Z\right), \end{aligned} \tag{26a}$$

$$P^1 = -(H+Z)H_X. \tag{26b}$$

The detailed calculations of the above leading-order and first-order solutions are illustrated in Appendix A.

Using the continuity equation, kinematic condition Eq. (23d) can be written in the conservation form

$$H_\tau + \partial_X \int_0^H U\,{\rm d}Z = 0. \tag{27}$$

Substituting $U = U^0 + \varepsilon U^1$ into Eq. (27), we obtain the equation

$$\begin{aligned} & H_\tau + H^2H_X + \varepsilon\left[Re\gamma\left(\frac{5}{6}H^4H_X + \frac{1}{2}H^2H_\tau\right)\right. \\ & - Re\left(\frac{3}{40}H^6H_X + \frac{5}{24}H^4H_\tau\right) + \frac{1}{3}\cot\alpha H^3H_X \\ & \left. + \frac{1}{2}Ma(\theta_{\rm i}^0-\theta_0)\theta_{{\rm i}X}^0 H^2 + \frac{1}{3}\varepsilon^2 WeH^3H_{XXX}\right]_X = 0. \end{aligned} \tag{28}$$

To eliminate the term of H_τ in Eq. (28), we only consider the zero-order solution, obtaining $H_\tau = -H^2H_X + O(\varepsilon)$ and applying it to Eq. (28). Following the transformation of $\varepsilon(\partial\tau, \partial X) \to (\partial\tau, \partial X)$, a new nonlinear evolution equation for the thin viscoelastic self-rewetting fluid film thickness is generated

$$\begin{aligned} & H_\tau + \underbrace{H^2H_X}_{\rm I} + \left[\underbrace{\frac{1}{3}Re\gamma H^4H_X}_{\rm II} + \underbrace{\frac{2}{15}ReH^6H_X}_{\rm III} \right. \\ & \left. + \underbrace{\frac{1}{3}\cot\alpha H^3H_X}_{\rm IV} - \underbrace{\frac{MaBi}{2(1+BiH)^2}(\theta_{\rm i}^0-\theta_0)H^2H_X}_{\rm V} \right. \\ & \left. + \underbrace{\frac{1}{3}WeH^3H_{XXX}}_{\rm VI}\right]_X = 0, \end{aligned} \tag{29}$$

where term I represents the convective term due to mean flow under the gravity component parallel to the substrate, term II corresponds to the viscoelastic effect, term III denotes the fluid inertia, term IV is the gravity component perpendicular to the substrate, term V accounts for the thermocapillary stress due to the interfacial temperature gradient, and term VI indicates the surface-tension effect. We adopt the viscoelastic parameter $\gamma_0 = 0.04$ N·s^2/m^2 of a typical Walters B$''$ fluid, and its dimensionless range is 0 to 0.4.[50,51] Therefore, our analysis of RT instability of viscoelastic self-wetting film is limited to theoretical aspects.

2.4. Linear stability analysis

To study the linear stability of the base state, the film thickness H is decomposed into its base solution $H = 1$ with a small spatiotemporal-dependent perturbation H^*, which reads

$$H = 1 + H^*. \tag{30}$$

After inserting Eq. (30) into Eq. (29) and ignoring all the nonlinearized terms of H^*, we obtain the following linear equation for the perturbation:

$$\begin{aligned} & H_\tau^* + H_X^* + \left[\frac{1}{3}Re\gamma H_X^* + \frac{2}{15}ReH_X^* + \frac{1}{3}\cot\alpha H_X^* \right. \\ & \left. - \frac{MaBi}{2(1+BiH)^2}(\theta_{\rm i}^0-\theta_0)H_X^* + \frac{1}{3}WeH_{XXX}^*\right]_X = 0. \end{aligned} \tag{31}$$

We assume a sinusoidal film perturbation of the form

$$H^* = \tilde{H}\exp({\rm i}kx + \omega\tau), \tag{32}$$

where ${\rm i}^2 = -1$, and ω, k, and $\tilde{H}$ ($\tilde{H} \ll 1$) denote complex wave frequency, the complex wave number, and amplitude of the perturbation, respectively. Substituting Eq. (32) into Eq. (31), we derive the general dispersion relation $\omega(k)$,

$$\begin{aligned} \omega = {} & -{\rm i}k + \frac{1}{3}Re\gamma k^2 + \frac{2}{15}Rek^2 + \frac{1}{3}\cot\alpha k^2 \\ & - \frac{MaBi}{2(1+Bi)^2}\Theta k^2 - \frac{1}{3}k^4 We, \end{aligned} \tag{33}$$

where $\omega = \omega_{\rm r} + {\rm i}\,\omega_i$ is the complex frequency, the real part $\omega_{\rm r}$ quantifies the advection of the perturbed wave and the imaginary part ω_i quantifies the temporal growth of the perturbation. Because the surface tension depends on the difference between the temperature corresponding to the minimum surface tension

θ and the interfacial temperature θ_i, we define a thermal parameter $\Theta = \theta_i - \theta_0$ to indicate the temperature difference for clarity. Therefore, in this linearized system, $\Theta > 0$ and $\Theta < 0$ correspond to $\theta_i > \theta_0$ and $\theta_i < \theta_0$ respectively, representing heating and cooling of plate. It is in the range of -1 to 1.[52]

According to Eq. (33), we obtain

$$\omega_r = \frac{1}{3}Re\gamma k^2 + \frac{2}{15}Rek^2 + \frac{1}{3}\cot\alpha k^2 - \frac{MaBi}{2(1+Bi)^2}\Theta k^2 - \frac{1}{3}k^4 We. \tag{34}$$

Positive values of ω_r indicate temporally instability and negative values of ω_r are stability, and the cutoff wavenumber k_c at $\omega_r = 0$ is

$$k_c = \sqrt{\frac{1}{We}\left(Re\gamma + \frac{2}{5}Re + \cot\alpha - \frac{3MaBi}{2(1+Bi)^2}\Theta\right)}. \tag{35}$$

By setting $\mathrm{d}\omega_r/\mathrm{d}k = 0$, we derive the wave number of the most unstable mode k_m,

$$k_m = \sqrt{\frac{1}{We}\left(\frac{1}{2}Re\gamma + \frac{1}{5}Re + \frac{1}{2}\cot\alpha - \frac{3MaBi}{4(1+Bi)^2}\Theta\right)}. \tag{36}$$

From Eqs. (35) and (36), we can clearly see that in the absence of substrate heating or cooling, namely, $\Theta = 0$, k_c, and k_m are strictly positive, indicating that the flow is always temporally unstable under an inclined plane ($0 < \alpha < \pi/2$). Due to the amplification of long waves by the gravitational component perpendicular to the substrate, unconditional instability is caused, *i.e.*, the $g\cos\alpha$ triggers the well-known Rayleigh–Taylor instability.[1,3]

Figure 3 depicts the variation of the real temporal growth rate ω_r with the wave number k when the viscoelastic coefficient γ changes in a heated and cooled substrate. The curves corresponding to viscoelastic self-rewetting fluids always lie above the curves associated with Newton liquid, and the curve with stronger viscoelastic coefficient is farther away from the Newton liquid curve, as can be seen from the two graphs. In other words, the cutoff wave number k_c and maximal growth rate ω_m increases with viscoelastic coefficient increases. Closer investigation reveals that the growth rate indicated in Fig. 3(a) is smaller than that seen in Fig. 3(b) for the same viscoelastic coefficient, revealing that the thermocapillary stress destabilizes the flow for a negative Θ. This conclusion is in agreement with case of self-rewetting films flowing down a vertical fiber ignoring the γ.[52]

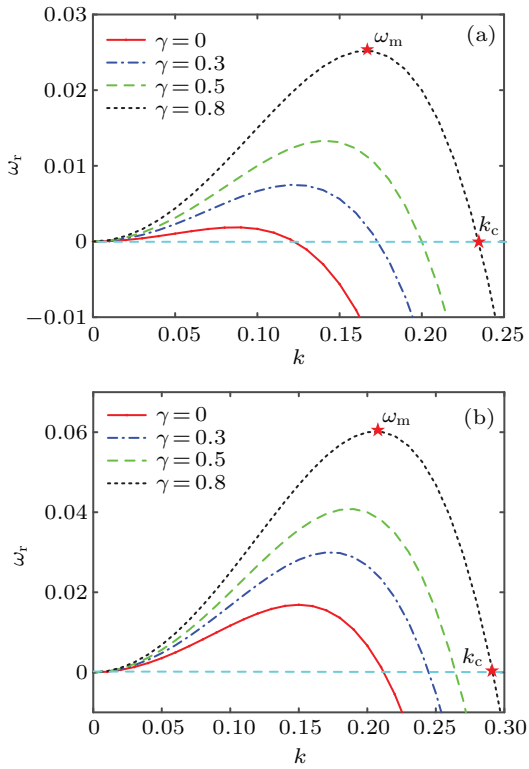


Fig. 3. Temporal growth rate ω_r as a function of wave number k for different γ: (a) a higher interfacial temperature, $\Theta = 1$; (b) a lower interfacial temperature, $\Theta = 1$. The results for a normal film ($\gamma = 0$) are also depicted for reference. Here, $\alpha = \pi/4$, $We = 100$, $Bi = 1$, $Ma = 4$, and $Re = 5$.

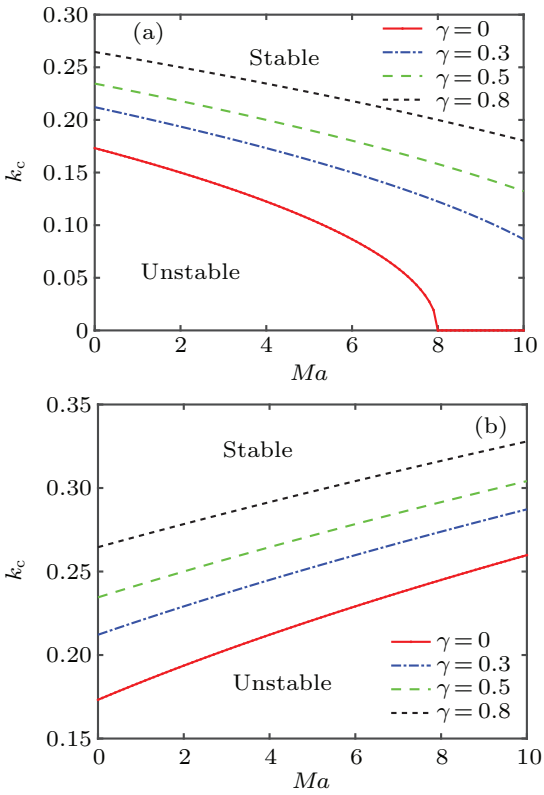


Fig. 4. Marginal stability curves demarcating the stable and unstable regions in the Ma–k_c plane when $\gamma = 0$, 0.3, 0.5, and 0.8 for a film under (a) a heated substrate ($\Theta > 0$) and (b) a cooled substrate ($\Theta < 0$). Here, $\alpha = \pi/4$, $We = 100$, $Bi = 1$, and $Re = 5$.

The curves displayed in Fig. 4 present the marginal stability curves as a function of the Marangoni number for different

values of viscoelastic parameter γ. For a given Ma, the linear unstable zone grows with rising γ in the vicinity of the threshold of instability, demonstrating that a lower viscoelastic coefficient stabilizes the film more effectively. In Fig. 4(a), we can clearly see that increasing Ma, the unstable regions decrease in the case of $\Theta > 0$. This result is totally opposite to the case of normal fluids in Ref. [17]. However, as seen in Fig. 4(b), the situation changes when Ma is increased. This is because the surface tension of self-wetting fluid is a monotonically decreasing function like that of ordinary fluid before the critical temperature $\theta_{\rm i}$, while it is a monotonically increasing function after the critical temperature $\theta_{\rm i}$. As for $\Theta < 0$, the interfacial temperature ($\theta_{\rm i}$) is lower than θ, where surface tension decreases as temperature increases, and thus Marangoni stresses exhibit the same properties as it in normal fluid. Also, it can be inferred from Fig. 4(a) the temporal RT instability is completely inhibited, when the Marangoni number Ma is greater than a critical value Ma. This result is consistent with an earlier study on hot capillary membranes.[53] More crucially, the critical value Ma increases with γ.

3. Numerical simulation

Since the nonlinear evolution equation of the film thickness is difficult to be solved analytically, numerical methods are needed to solve the Eq. (29). We employ the line approach to numerically solve the nonlinear equations in order to better understand the space–time dynamics.[54] A perturbation with the most unstable wave number $k_{\rm m}$ is utilized as the initial condition

$$H = 1 + 0.05\cos k_{\rm m} x. \tag{37}$$

The detailed algorithm of the line method is illustrated in Appendix B.

To verify the availability of the present code, we compared the nonlinear evolution equation with the results obtained by Jia and Jian in Ref. [55]. Since the expression of the surface tension is different, we should select the first half of the quadratic function, namely $\theta_{\rm i} < \theta_0$. Since $\Theta = \theta_{\rm i} - \theta_0$, for the simplified model, let us say $\Theta = -1$. When $\gamma = 0$, $\Theta = -1$, we plot Fig. 5, which shows that we have a good agreement with Jia and Jian.[55]

Figure 6 respectively describes the free surface thickness H of Eqs. (31) and (29) under cooling and heating conditions. We can observe small amplitude fluctuation of the free surface thickness H, which is consistent with the small amplitude disturbance considered by linear stability method and long wave approximation method. However, it is worth noting that the amplitude fluctuation of the numerical simulation is more violent than that of the linear stabilization method, and the peak value moves slightly to the upstream of the substrate. And it is even more pronounced under cooling conditions. But the overall trend of evolution of the two free surfaces is the same.

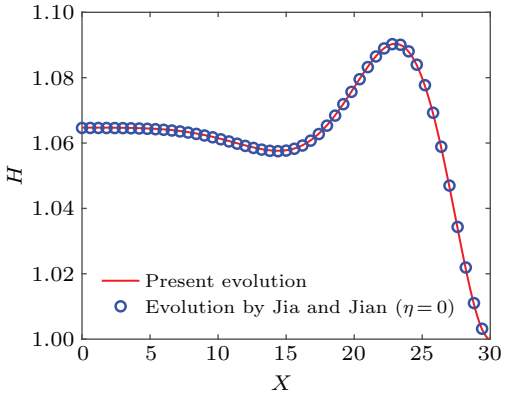


Fig. 5. Comparisons of the evolution of free surface thickness H of Jia and Jian[55] and the present study by setting some dimensionless parameters $Re = 1$, $Ma = 3$, $Bi = 1$, $\alpha = \pi/4$, $We = 30$, $t = 30$.

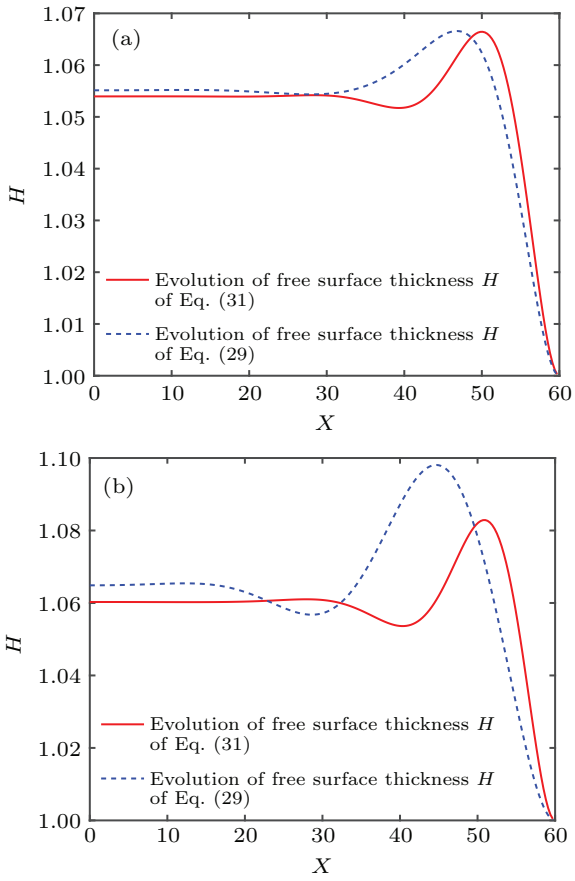


Fig. 6. Comparisons of the evolution of free surface thickness H of Eqs. (31) and (29) by setting some dimensionless parameters $Re = 3$, $Ma = 3$, $Bi = 1$, $\alpha = \pi/4$, $We = 100$, $t = 50$, $\gamma = 0.2$. Different panels in the graphs indicate (a) $\Theta = 1$, (b) $\Theta = -1$.

In Figs. 7 and 8, we describe the temporal evolutions of the thin film at sequenced time scales t = 10–30 under the conditions of substrate heating and cooling respectively. Figure 7(a) shows that the wave amplitude is less than 1.06 and the frequency is quite slow for $\gamma = 0$. To investigate the influence of the viscoelastic coefficient γ on the film instability, we increase γ from 0 to 0.4 in Figs. 7(b)–7(d). We find that the amplitude and frequency of waves increase with the increase

of γ. Similarly, we can also clearly find same conclusion from the changes in Fig. 8. It is worth noting that when $\Theta = -1$, the wave frequency and amplitude are significantly enhanced compared with that when $\Theta = 1$ under the same conditions. It is further verified that substrate heating has an inhibitory effect on RT instability.

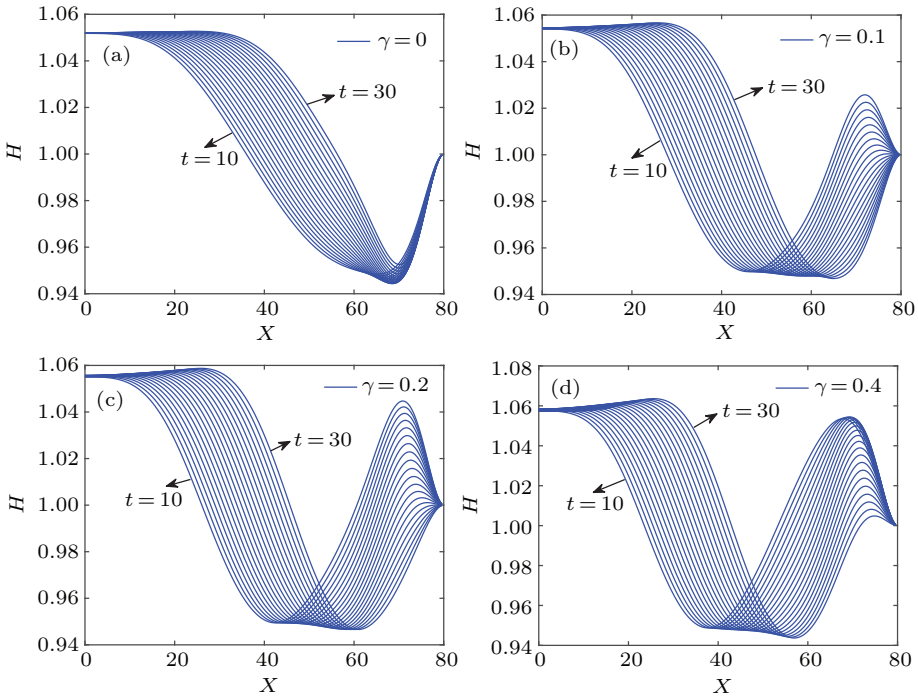


Fig. 7. The film thickness for different time scales, when $Re = 3$, $We = 100$, $Bi = 1$, $\alpha = \pi/4$, $Ma = 3$, $t = 10$–30, $\Theta = 1$. Different panels in the graphs indicate (a) $\gamma = 0$, (b) $\gamma = 0.1$, (c) $\gamma = 0.2$, (d) $\gamma = 0.4$.

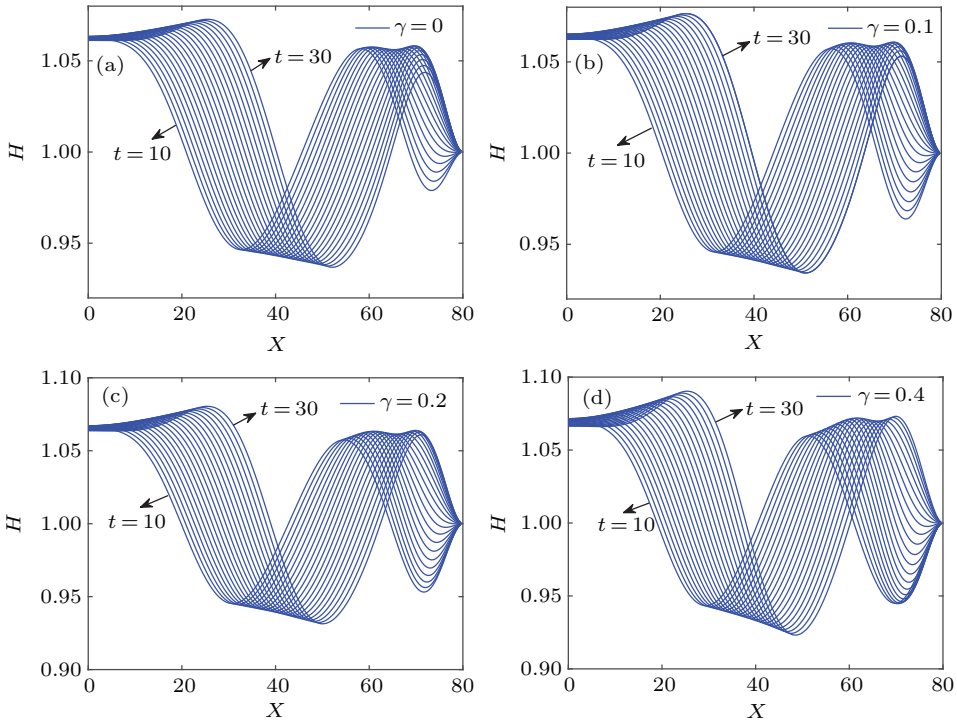


Fig. 8. The film thickness for different time scales, when $Re = 3$, $We = 100$, $Bi = 1$, $\alpha = \pi/4$, $Ma = 3$, $t = 10$–30, $\Theta = -1$. Different panels in the graphs indicate (a) $\gamma = 0$, (b) $\gamma = 0.1$, (c) $\gamma = 0.2$, (d) $\gamma = 0.4$.

Figures 9 and 10 represent long-time free surface evolution for different viscoelastic coefficients γ. The subplots describe the 60–80 time span when $\Theta = 1$ and $\Theta = -1$. The wave crests magnify as the increase of viscoelastic coefficient, confirming its destabilizing effect. By observing Figs. 9 and 10 at the same time, we can demonstrate again the promoting effect of $\Theta < 0$ on RT instability. A comparison between Figs. 7, 8, and 9, 10 demonstrates that the wave amplitude

increases dramatically as t increases. In addition, oscillation of the thin liquid film tends to accumulate downstream of the tilted substrate under long periods of oscillation, and the free surface is flat in the front end of substrate. Further, we investigate the combined effects of γ and Θ in Figs. 9(a) and 10(d). Comparing Fig. 9(a) with Fig. 10(d), we can clearly see that RT instability becomes more unstable with γ increases, as Θ changes from heated to cooled.

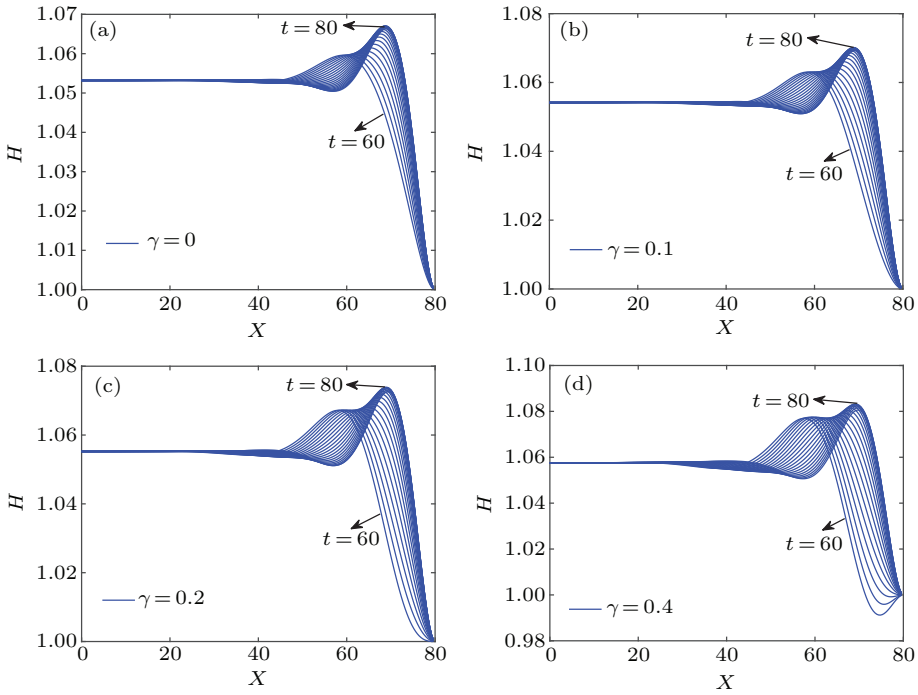


Fig. 9. The film thickness for different time scales, when $Re=3$, $We=100$, $Bi=1$, $\alpha=\pi/4$, $Ma=3$, $t=60$–80, $\Theta=1$. Different panels in the graphs indicate (a) $\gamma=0$, (b) $\gamma=0.1$, (c) $\gamma=0.2$, (d) $\gamma=0.4$.

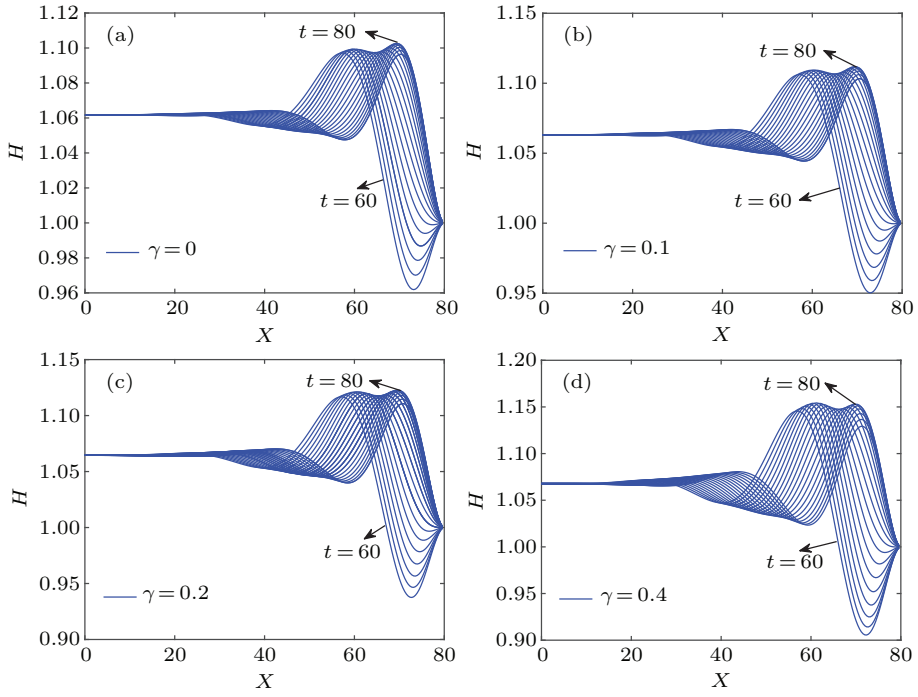


Fig. 10. The film thickness for different time scales, when $Re=3$, $We=100$, $Bi=1$, $\alpha=\pi/4$, $Ma=3$, $t=60$–80, $\Theta=-1$. Different panels in the graphs indicate (a) $\gamma=0$, (b) $\gamma=0.1$, (c) $\gamma=0.2$, (d) $\gamma=0.4$.

Typical results of the numerical solution of the self-rewetting viscoelastic liquid under an inclined plane are presented in Figs. 11 and 12. Here, we describe the free surface configurations at an instant $t=50$. A comparison between the Figs. 11(a) and 11(b) shows that decreasing Re stabilizes the flow by weakening the wave amplitude when fixing other parameters constant. This means that the effect of inertia on flow stability is significant. From Fig. 11(c), we observe that

for any given γ, the wave amplitude increases with decreasing *We*, which clearly detects the stabilizing role of the Weber number *We*. Because a large value of the Weber number corresponds to large surface tension, the surface instability will be impeded if a larger Weber number is used. Taking Figs. 11(a) and 11(d) into consideration, the amplitude of the perturbation shrinks with increasing α, indicating that a larger inclination angle stabilizes the film more strongly. This is because gravity tangential component causes a flow that might influence the disturbance, allowing the instability to shift partially at small inclinations but totally disappear at larger inclinations. The analysis results in Fig. 12 are the same as those in Fig. 11, which are only two cases of substrate heating and cooling.

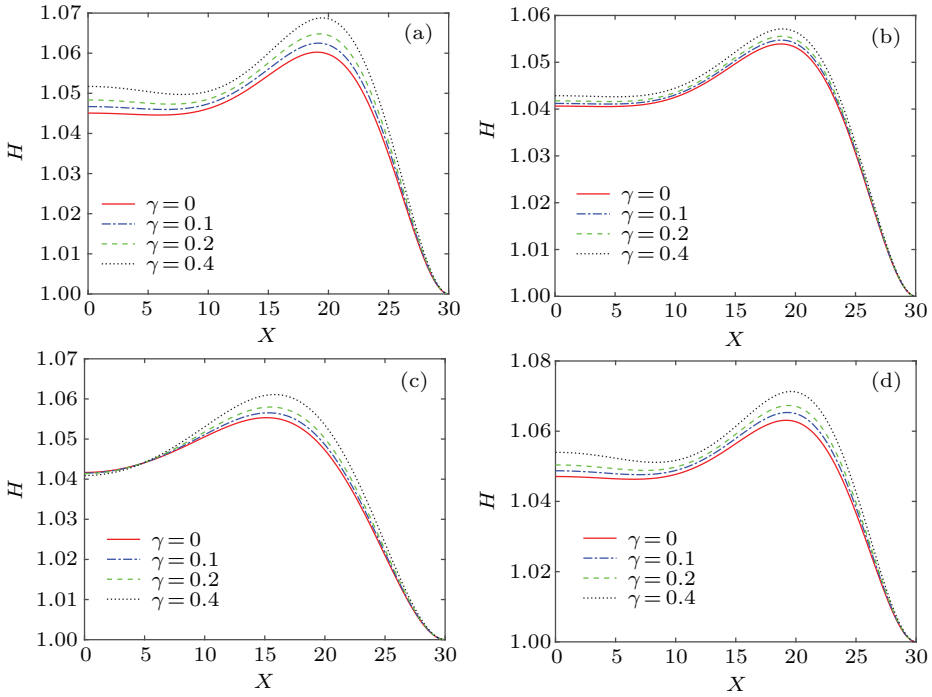


Fig. 11. The film thickness for different viscoelastic coefficients at $X = 0 \sim 30$, when $Ma = 3$, $\Theta = 1$, $t = 50$, $Bi = 1$. Different panels in the graphs indicate (a) $Re = 3$, $We = 100$, $\alpha = \pi/4$; (b) $Re = 1$, $We = 100$, $\alpha = \pi/4$; (c) $Re = 3$, $We = 250$, $\alpha = \pi/4$; (d) $Re = 3$, $We = 100$, $\alpha = \pi/5$.

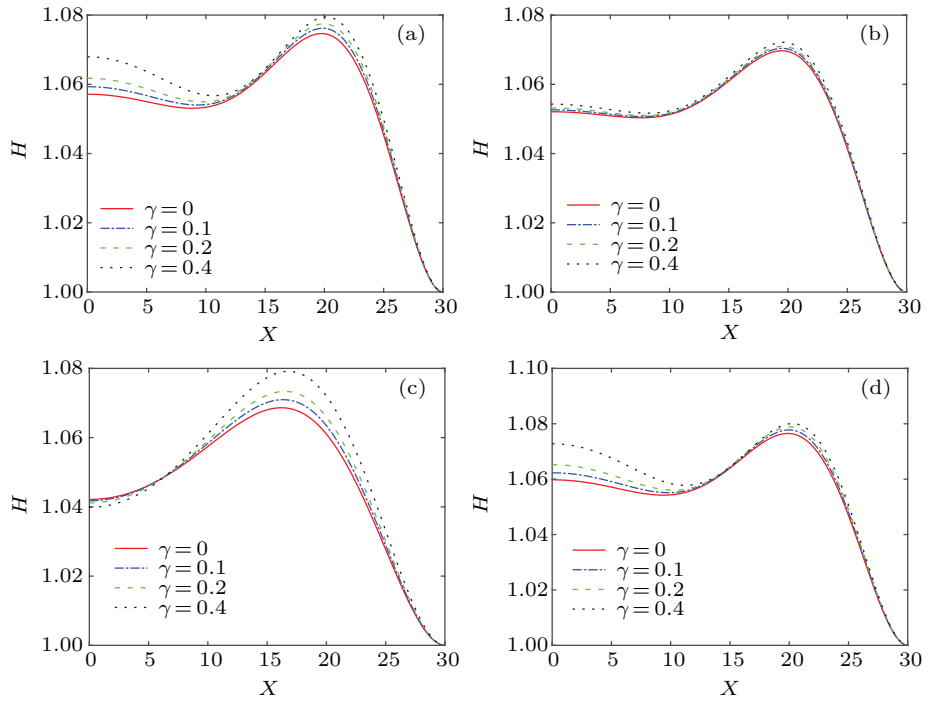


Fig. 12. The film thickness for different viscoelastic coefficients at $X = 0 \sim 30$, when $Ma = 3$, $\Theta = -1$, $t = 50$, $Bi = 1$. Different panels in the graphs indicate (a) $Re = 3$, $We = 100$, $\alpha = \pi/4$; (b) $Re = 1$, $We = 100$, $\alpha = \pi/4$; (c) $Re = 3$, $We = 250$, $\alpha = \pi/4$; (d) $Re = 3$, $We = 100$, $\alpha = \pi/5$.

Figures 13 and 14 also give the typical results of numerical solutions of the self-rewetting viscoelastic liquid under an inclined substrate. But the length of the substrate X is different from Figs. 11 and 12. The length of the substrate in Figs. 11 and 12 is $X = 30$, and the length of the substrate in Figs. 13 and 14 is $X = 60$. Comparing Figs. 11 and 13, we find that the longer substrate, the less obvious the fluctuation in the upstream of the substrate. At the same time, the crest will move downstream as the substrate grows. It is worth noting that increasing the substrate length results in an increase in amplitude of the perturbation. This means that the RT instability is promoted with plate length.

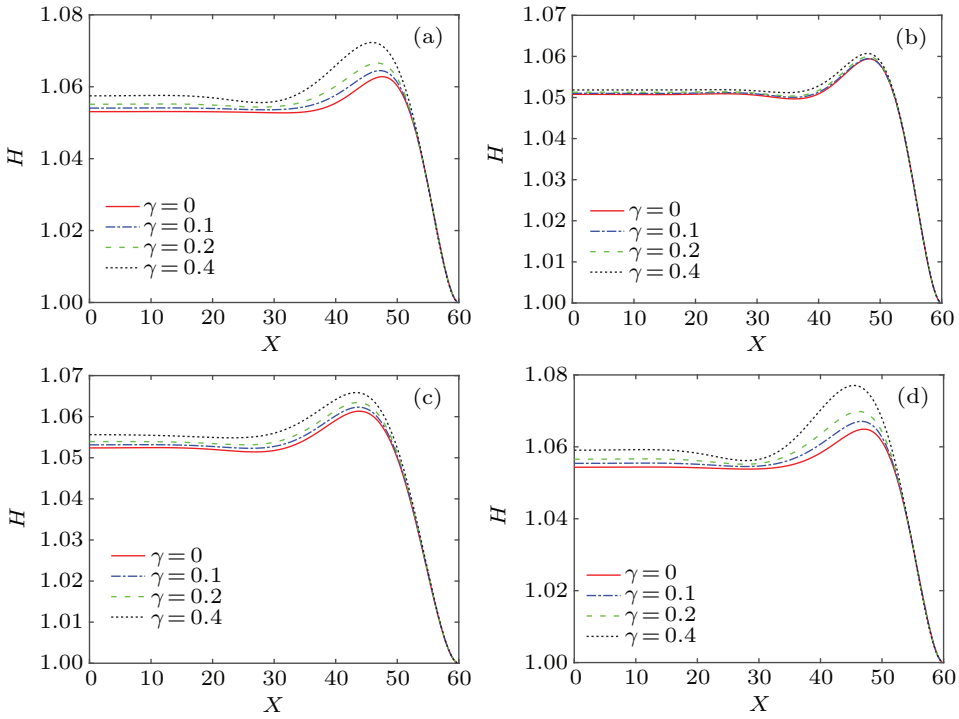


Fig. 13. The film thickness for different viscoelastic coefficients at $X = 0 \sim 60$, when $Ma = 3$, $\Theta = 1$, $t = 50$, $Bi = 1$. Different panels in the graphs indicate (a) $Re = 3$, $We = 100$, $\alpha = \pi/4$; (b) $Re = 1$, $We = 100$, $\alpha = \pi/4$; (c) $Re = 3$, $We = 250$, $\alpha = \pi/4$; (d) $Re = 3$, $We = 100$, $\alpha = \pi/5$.

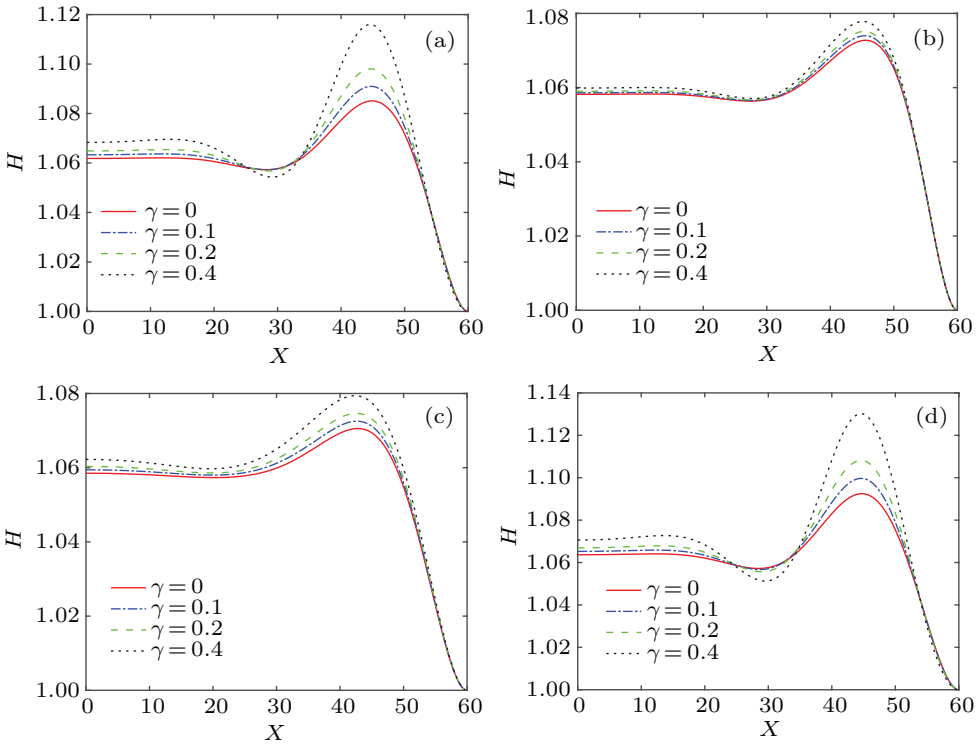


Fig. 14. The film thickness for different viscoelastic coefficients at $X = 0 \sim 60$, when $Ma = 3$, $\Theta = -1$, $t = 50$, $Bi = 1$. Different panels in the graphs indicate (a) $Re = 3$, $We = 100$, $\alpha = \pi/4$; (b) $Re = 1$, $We = 100$, $\alpha = \pi/4$; (c) $Re = 3$, $We = 250$, $\alpha = \pi/4$; (d) $Re = 3$, $We = 100$, $\alpha = \pi/5$.

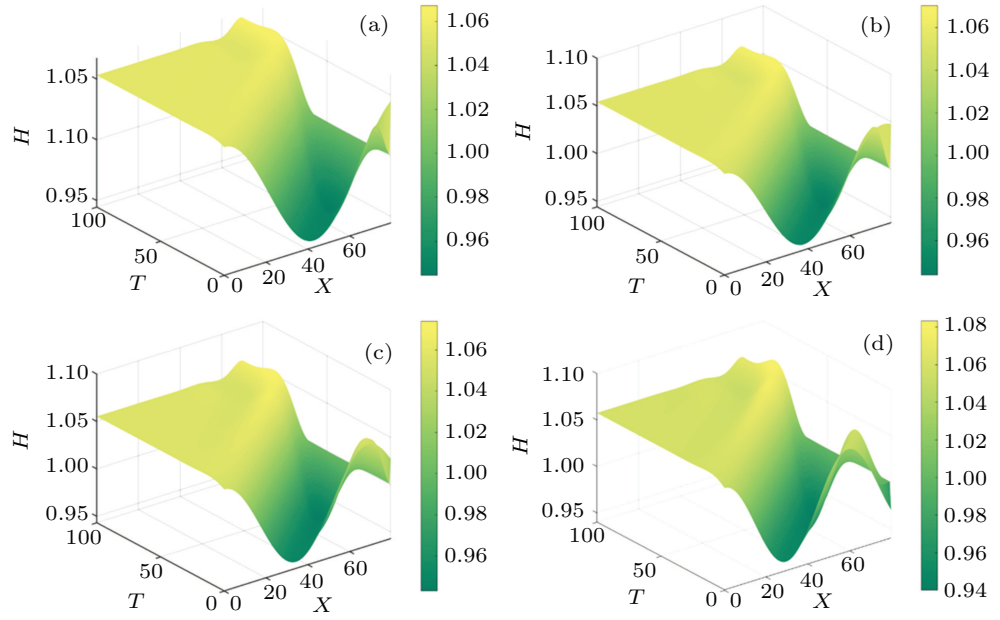


Fig. 15. Three-dimensional view of the waves with fixed $Re = 3$, $We = 100$, $Bi = 1$, $Ma = 3$, $\Theta = 1$, and $\alpha = \pi/4$. Different panels in the graphs indicate (a) $\gamma = 0$, (b) $\gamma = 0.1$, (c) $\gamma = 0.2$, (d) $\gamma = 0.4$.

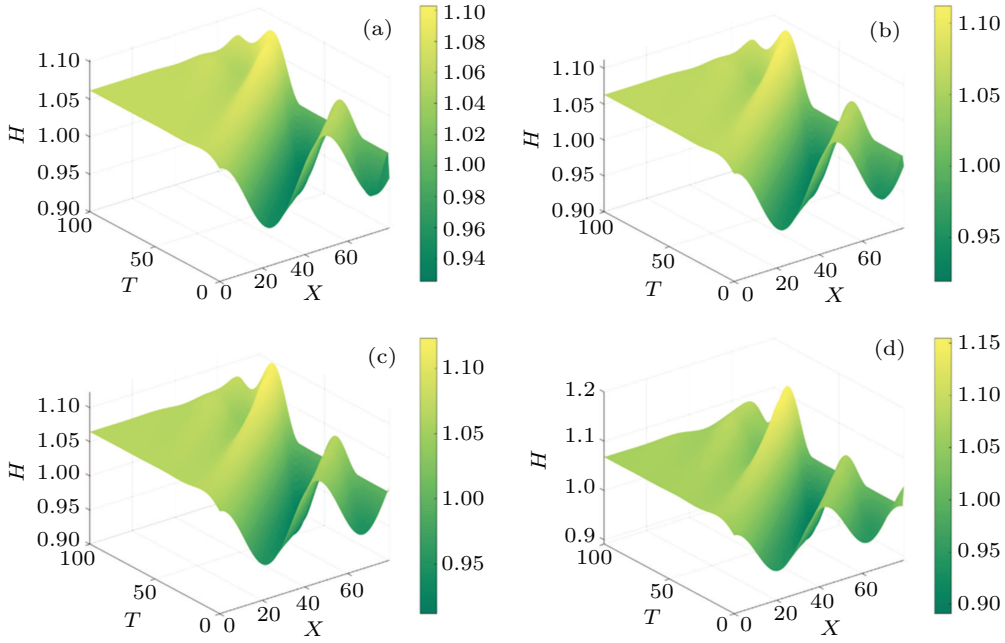


Fig. 16. Three-dimensional view of the waves with fixed $Re = 3$, $We = 100$, $Bi = 1$, $Ma = 3$, $\Theta = -1$, and $\alpha = \pi/4$. Different panels in the graphs indicate (a) $\gamma = 0$, (b) $\gamma = 0.1$, (c) $\gamma = 0.2$, (d) $\gamma = 0.4$.

Figures 15 and 16 display the evolution of the wave with X and T for different viscoelastic parameters γ under cooling and heating. All the figures demonstrate that the wave's maximum height and wave frequency increase with an increase in γ.

4. Conclusions

To summarize, in this work we have developed and investigated for Rayleigh Taylor instability of viscoelastic self-rewetting film flows under a temperature-controlled inclined substrate. The rheological property of the viscoelastic liquid is described by Walters B$''$ model. The nonlinear free surface evolution equation is derived from the governing equations and boundary conditions and the viscoelastic parameter γ is introduced to characterize the viscoelastic effect. The heated capillary stress makes the flow unstable when Θ is negative, regardless of whether the viscoelastic effect is incorporated, according to the linear stability of the evolution equation. But when Θ is positive, the heated capillary stress makes the flow more stable. Furthermore, analysis of the dispersion relation showed that whenever $\Theta > 0$ or $\Theta < 0$, the real temporal growth rate and cutoff wave number increase with the

increase of viscoelastic coefficient. By comparing $\Theta > 0$ and $\Theta < 0$, we found that the actual time growth rate and cutoff wave number increase more significantly at $\Theta < 0$. Moreover, we use the line method to numerically simulate the nonlinear evolution equation and systematically examine the space-time variation of the film free surface. The numerical results reveal that the magnitude and frequency of the disturbance increase with the viscoelastic coefficient. The numerical simulation results also found that thin liquid film oscillation tends to accumulate downstream of the inclined substrate when the evolution time is long enough. Also, we found that increasing *We* or α makes the system more stable for a given range of viscoelastic coefficients. However, increasing *Re* shows the opposite result. At the same time, we can also found that the length of the substrate also promotes RT instability.

Appendix A: Derivation of leading-order and first-order solutions

In this paper, we only consider the first-order $O(\varepsilon)$ model, in which the governing equation Eq. (21) and the associated boundary condition Eqs. (22) and (23) become

$$U_X + W_Z = 0, \tag{A1a}$$

$$\begin{aligned}&\varepsilon Re(U_\tau + UU_X + WU_Z)\\ &= 1 - \varepsilon P_X + U_{ZZ} - \gamma Re\varepsilon(U_{ZZ\tau} - UW_{ZZZ}\\ &\quad + WU_{ZZZ} + W_{ZZ}U_Z - W_Z U_{ZZ}),\end{aligned} \tag{A1b}$$

$$\cot\alpha - P_Z + \varepsilon W_{ZZ} = 0, \tag{A1c}$$

$$\theta_{ZZ} = 0. \tag{A1d}$$

At $Z = 0$,

$$U = 0, \quad W = 0, \quad \theta = 1, \tag{A2}$$

and at $Z = H$,

$$\begin{aligned}&-P - 2\varepsilon(U_X + H_X U_Z)\\ &= [We + \frac{1}{2}Ma(\theta_\mathrm{i} - \theta_0)^2]\varepsilon^2 H_{XX},\end{aligned} \tag{A3a}$$

$$\begin{aligned}&U_Z - Re\gamma\varepsilon(2H_X U_Z^2 + U_{Z\tau} + UU_{XZ} + WU_{ZZ}\\ &\quad - 2U_Z W_Z) = Ma(\theta_\mathrm{i} - \theta_0)\varepsilon\theta_{\mathrm{i},X},\end{aligned} \tag{A3b}$$

$$\theta_{\mathrm{i},Z} = -Bi\theta_\mathrm{i}. \tag{A3c}$$

As mentioned above, all variables $[U, W, P, \theta]$ are expanded to

$$\begin{aligned}&[U, W, P, \theta]\\ &= [U^0, W^0, P^0, \theta^0] + \varepsilon[U^1, W^1, P^1, \theta^1] + O(\varepsilon^2),\end{aligned} \tag{A4}$$

which are inserted into Eqs. (A1a)–(A3a) to yield the zeroth-order and the first-order governing equations.

(i) Zeroth-order equations

$$\begin{aligned}&U_X^0 + W_Z^0 = 0, \quad U_{ZZ}^0 = -1, \quad P_Z^0 = \cot\alpha, \quad \theta_{ZZ}^0 = 0,\\ &Z = 0: \quad U^0 = 0, \quad W^0 = 0, \quad \theta^0 = 1,\\ &Z = H: \quad P^0 = -\left[We + \frac{1}{2}Ma(\theta_\mathrm{i}^0 - \theta_0)^2\right]\varepsilon^2 H_{XX},\\ &U_Z^0 = 0, \quad \theta_{\mathrm{i},Z}^0 = -Bi\theta_\mathrm{i}^0.\end{aligned}$$

(ii) Leading-order solutions

$$\begin{aligned}U^0 &= -\frac{1}{2}Z^2 + HZ,\\ W^0 &= -\frac{1}{2}H_X Z^2,\\ P^0 &= \cot\alpha(Z - H) - We\varepsilon^2 H_{XX}\\ &\quad - \frac{1}{2}Ma(\theta_\mathrm{i}^0 - \theta_0)^2\varepsilon^2 H_{XX},\\ \theta^0 &= 1 - \frac{BiZ}{1 + BiH}.\end{aligned}$$

The zeroth-order interfacial temperature: $\theta_\mathrm{i}^0 = \theta^0|_{Z=H} = 1/(1 + BiH)$.

(iii) First-order equations

$$\begin{aligned}&U_X^1 + W_Z^1 = 0,\\ &Re(U_\tau^0 + U^0 U_X^0 + W^0 U_Z^0)\\ &= -P_X^0 + U_{ZZ}^1 - \gamma Re(U_{ZZ\tau}^0 - U^0 W_{ZZZ}^0\\ &\quad + W^0 U_{ZZZ}^0 + W_{ZZ}^0 U_Z^0 - W_Z^0 U_{ZZ}^0),\\ &-P_Z^1 + W_{ZZ}^0 = 0,\\ &\theta_{ZZ}^1 = 0,\\ &Z = 0: \quad U^1 = 0, \; W^1 = 0, \; \theta^1 = 0,\\ &Z = H: \quad P^1 + 2(U_X^0 + H_X U_Z^0) = 0, \; \theta_{\mathrm{i},Z}^1 = -Bi\theta_\mathrm{i}^1,\\ &U_Z^1 - Re\gamma[2H_X(U_Z^0)^2 + U_{Z\tau}^0\\ &\quad + U^0 U_{XZ}^0 + W^0 U_{ZZ}^0 - 2U_Z^0 W_Z^0]\\ &= Ma(\theta_\mathrm{i}^0 - \theta_0)\theta_{\mathrm{i},X}^0.\end{aligned}$$

(iv) First-order solutions

$$\begin{aligned}U^1 &= \left[\cot\alpha H_X + \varepsilon^2 WeH_{XXX} + \frac{1}{2}Ma(\theta_\mathrm{i}^0 - \theta_0)^2\varepsilon^2 H_{XXX}\right.\\ &\quad \left. + Ma(\theta_\mathrm{i}^0 - \theta_0)\theta_{\mathrm{i},X}^0\varepsilon^2 H_{XX}\right](HZ - \frac{Z^2}{2}) + Ma(\theta_\mathrm{i}^0\\ &\quad - \theta_0)\theta_{\mathrm{i},X}^0 Z + Re\left(\frac{Z^3}{6}H_\tau - \frac{Z}{2}H^2 H_\tau - \frac{Z}{6}H^4 H_X + \frac{Z^4}{24}HH_X\right)\\ &\quad - Re\gamma\left(\frac{Z^2}{2}HH_X - H_\tau Z - 2H^2 H_X Z\right),\\ P^1 &= -(H + Z)H_X.\end{aligned}$$

Appendix B: Numerical simulation

To better solve this problem, equation (29) should be rewritten as

$$\frac{\partial H}{\partial T} + \frac{\partial Q}{\partial X} = 0, \tag{B1}$$

with

$$Q = \frac{1}{3}H^3 + \frac{1}{3}\cot\alpha H^3 H_X + \frac{1}{3}WeH^3 H_{XXX} - \frac{1}{2}\frac{MaBi\Theta}{(1+BiH)^2}H^2 H_X + \frac{2}{15}ReH^6 H_X + \frac{1}{3}Re\gamma H^4 H_X. \tag{B2}$$

Since equation (B1) is a fourth-order partial differential equation, four boundary conditions and an initial condition are required. When the liquid–gas interface is in contact with a solid, previous careful experimental studies of the contact line region show that true contact is not really achieved. Instead, the surface of what appears to be a dry solid is covered by a very thin film called lead film.[54] In this work, the precursor film is defined at downstream ($X = L$) and the thickness does not change with time. Therefore, the four boundary conditions are

$$H(L,T) = 1, \quad \frac{\partial H}{\partial X}(L,T) = 0, \quad \frac{\partial H}{\partial X}(0,T) = 0, \quad \frac{\partial^3 H}{\partial X^3}(0,T) = 0, \tag{B3}$$

where L denotes the nondimensional domain length. We use the unified spatial grid $X_i = (i-1)\Delta X$, $i = 1,\ldots,N$ to discretize nonlinear evolution equation, where $X = L/N$. The film thickness values at the grid points, denoted by H_i, are functions of time only and satisfy a system of N first-order ordinary differential equations

$$\frac{\partial H_i}{\partial T} = -\frac{Q_{i+1/2} - Q_{i-1/2}}{\Delta X}, \tag{B4}$$

where $Q_{i\pm1/2}$ are values of Q at points half-way between i and $i\pm1$ the grid points, $X_{i\pm1/2} = X_i \pm \Delta X/2$. When the index i is between 3 and $N-2$, $Q_{i\pm1/2}$ are expressed as

$$\begin{aligned} Q_{i+1/2} = {} & \frac{1}{6}(H_{i+1}^3 + H_i^3) + \frac{1}{6}\cot\alpha(H_{i+1}^3 + H_i^3)\frac{H_{i+1} - H_i}{\Delta X} \\ & + \frac{1}{6}We(H_{i+1}^3 + H_i^3)\frac{H_{i+2} - 3H_{i+1} + 3H_i - H_{i-1}}{\Delta X^3} \\ & - \frac{1}{4}\frac{MaBi\Theta}{(1+Bi(H_{i+1}+H_i)/2)^2}(H_{i+1}^2 + H_i^2)\frac{H_{i+1} - H_i}{\Delta X} \\ & + \frac{1}{15}Re(H_{i+1}^6 + H_i^6)\frac{H_{i+1} - H_i}{\Delta X} \\ & + \frac{1}{6}Re\gamma(H_{i+1}^4 + H_i^4) \times \frac{H_{i+1} - H_i}{\Delta X}, \end{aligned} \tag{B5}$$

$$\begin{aligned} Q_{i-1/2} = {} & \frac{1}{6}(H_i^3 + H_{i-1}^3) + \frac{1}{6}\cot\alpha(H_i^3 + H_{i-1}^3)\frac{H_i - H_{i-1}}{\Delta X} \\ & + \frac{1}{6}We(H_i^3 + H_{i-1}^3)\frac{H_{i+1} - 3H_i + 3H_{i-1} - H_{i-2}}{\Delta X^3} \\ & - \frac{1}{4}\frac{MaBi\Theta}{(1+Bi(H_i+H_{i-1})/2)^2}(H_i^2 + H_{i-1}^2)\frac{H_i - H_{i-1}}{\Delta X} \\ & + \frac{1}{15}Re(H_i^6 + H_{i-1}^6)\frac{H_i - H_{i-1}}{\Delta X} \\ & + \frac{1}{6}Re\gamma(H_i^4 + H_{i-1}^4) \times \frac{H_i - H_{i-1}}{\Delta X}. \end{aligned} \tag{B6}$$

It should be noted that in order to ensure that discretization is consistent with the mass conservation of the liquid, the function Q in Eq. (B4) should be evaluated at $i\pm1/2$ instead of $i\pm1$. For $i = 1$, 2, $N-1$, and N, this finite difference method,[53] which is second-order accurate in space, produces imaginary points (points outside the domain). Near $X = 0$, we use the symmetry condition to obtain $H_0 = H_2$ and $H_{-1} = H_3$. The first equation of Eq. (B3) indicates that the film is flat near $X = L$, so the thickness at the imaginary point corresponding to $i = N+2$ can be approximated by the zero-slope condition, resulting in $H_{N+2} = H_N$. Further, equation (B4) can be solved using a standard differential equation solver (for example, MATLAB software).

Acknowledgements

Project supported by the National Natural Science Foundation of China (Grant No. 1226 2026), the Natural Science Foundation of Inner Mongolia Autonomous Region of China (Grant No. 2021 MS01007), and the Inner Mongolia Grassland Talent, China (Grant No. 12000-12102013).

References

[1] Taylor G I 1950 *Proc. R. Soc. Lond. A* **201** 192
[2] Lewis D J 1950 *Proc. R. Soc. Lond. A* **202** 81
[3] Rayleigh L 1882 *Proc. Lond. Math. Soc.* **s1–14** 170
[4] Burgess J M, Juel A, McCormick W D, Swift J B and Swinney H L 2001 *Phys. Rev. Lett.* **86** 1203
[5] Seemann R, Herminghaus S, Neto C, Schlagowski S, Podzimek D, Konrad R, Mantz H and Jacobs K 2005 *J. Phys: Condens. Matter* **17** 267
[6] Haas F C 1964 *AICHE J.* **10** 920
[7] Stone H A, Stroock A D and Ajdari A 2004 *Annu. Rev. Fluid Mech.* **36** 381
[8] Vinningland J L, Johnsen Ø, Flekkøy E G, Toussaint R and Måløy K J 2007 *Phys. Rev. Lett.* **99** 048001
[9] Sharp D H 1984 *Physica D* **12** 3
[10] Kull H J 1991 *Phys. Rep.* **206** 197
[11] Tomlin R J, Cimpeanu R and Papageorgiou D T 2020 *Phys. Rev. Fluids* **5** 013703
[12] Sterman-Cohen E, Bestehorn M and Oron A 2017 *Phys. Fluids* **29** 052105
[13] Baldwin K A, Scase M M and Hill R J 2015 *Sci. Rep.* **5** 11706
[14] Alqatari S, Videbæk T E, Nagel S R, Hosoi A E and Bischofberger I 2020 *Sci. Adv.* **6** eabd6605
[15] Weidner D E, Schwartz L W and Eres M H 2007 *Chem. Prod. Process Model.* **2** 1
[16] Mikaelian K O 2016 *Phys. Rev. E* **93** 023104
[17] Scase M M and Hill R J A 2018 *J. Fluid Mech.* **852** 543
[18] Yiantsios S G and Higgins B G 1989 *Phys. Fluids A* **1** 1484
[19] Brun P T, Damiano A, Rieu P, Balestra G and Gallaire F 2015 *Phys. Fluids* **27** 084107
[20] Lister J R, Rallison J M and Rees S J 2010 *J. Fluid Mech.* **647** 239
[21] Chao Y C, Zhu L L and Yuan H 2021 *Phys. Rev. Fluids* **6** 064001
[22] Maxwell J C 1867 *Philos. Trans. R. Soc. Lond.* **157** 49
[23] Jeffreys H 1929 *The Earth*, 2nd edn. (Cambridge: Cambridge University Press)
[24] Giesekus H A 1982 *J. Non-Newton. Fluid Mech.* **11** 69
[25] Thien N P and Tanner R I 1977 *J. Non-Newton. Fluid Mech.* **2** 353
[26] Oldroyd J G 1950 *Philos. Trans. R. Soc. Lond.* **200** 523

[27] Boffetta G, Mazzino A, Musacchio S and Vozella L 2010 *J. Fluid Mech.* **643** 127
[28] Gou J N, Zan W T, Sun Y B, and Wang C 2021 *Phys. Rev. E* **104** 025110
[29] Bird R B, Armstrong R C and Hassager O 1987 *Dynamics of Polymeric Liquids* (Wiley: Wiley-Interscience)
[30] Fu Q F, Hu T and Yang L J 2018 *Phys. Fluids* **30** 084102
[31] Nadeem S, Akbar N S, Hayat T and Hendi A 2011 *Appl. Math. Mech.* **32** 689
[32] Waqas H, Alghamdi M, Muhammad T and Khan M A 2021 *Case Stud. Therm. Eng.* **26** 101097
[33] Khan M I, Khan S U, Jameel M, Chu Y M, Tlili I and Kadry S 2021 *Surf. Interfaces* **22** 100849
[34] Larson R G 1992 *Rheol. Acta* **31** 213
[35] Savins J G 1967 *Rheol. Acta* **6** 323
[36] Wei H H 2005 *Phys. Rev. E* **71** 066306
[37] Abe Y 2006 *Ann. NY Acad. Sci.* **1077** 650
[38] Karapetsas G, Sahu K C, Sefiane K and Matar O K 2014 *Langmuir* **30** 4310
[39] Mamalis D, Koutsos V and Sefiane K 2018 *Langmuir* **34** 1916
[40] Ye X, Zhang X, Li M and Li C 2018 *Phys. Fluids* **30** 112103
[41] Batson W, Agnon Y and Oron A 2017 *J. Fluid Mech.* **819** 562
[42] Ma C C and Liu J L 2021 *Phys. Fluids* **33** 022101
[43] Scholle M, Haas A, Aksel N, Thompson H, Hewson R and Gaskell P 2009 *Int. J. Heat Fluid Fl.* **30** 175
[44] Beard D W and Walters K 1964 *Math. Proc. Cambridge* **60** 667
[45] Bergman T L, Incropera F P, DeWitt D P and Lavine A S 2011 *Fundamentals of Heat and Mass Transfer*, 3rd edn. (New York: John Wiley & Sons)
[46] Chao Y, Lu Y and Yuan H 2020 *Int. J. Heat Mass Transfer* **147** 118942
[47] Li P and Chao Y C 2020 *Chem. Eng. Sci.* **227** 115936
[48] Mamalis D, Koutsos V and Sefiane K 2016 *Appl. Phys. Lett.* **109** 231601
[49] Yu Z 2018 *Phys. Fluids* **30** 082104
[50] Hayat T, Asad S, Mustafa M and Alsulami H H 2014 *Chin. Phys. B* **23** 084701
[51] Mohammed Rizwan Sadiq I and Usha R 2005 *Int. J. Eng. Sci.* **43** 1435
[52] Ma C C, Liu J L, Dai X J and Liu Y Q 2022 *Eur. J. Mech. B-Fluid* **91** 152
[53] Deissler R J and Oron A 1992 *Phys. Rev. Lett.* **68** 2948
[54] Ajaev V S 2012 *Interfacial Fluid Mechanics* (Springer: Springer Boston MA)
[55] Jia B N and Jian Y J 2022 *Phys. Fluids* **34** 044104